

# Quantum statistics of atoms in microstructures

Erika Andersson, Márcia T. Fontenelle and Stig Stenholm

*Department of Physics, Royal Institute of Technology, Lindstedtsv. 24, SE-10044 Stockholm, Sweden*  
(April 28, 2018)

This paper proposes groove-like potential structures for the observation of quantum information processing by trapped particles. As an illustration the effect of quantum statistics at a 50-50 beam splitter is investigated. For non-interacting particles we regain the results known from photon experiments, but we have found that particle interactions destroy the perfect bosonic correlations. Fermions avoid each other due to the exclusion principle and hence they are far less sensitive to particle interactions. For bosons, the behavior can be explained with simple analytic considerations which predict a certain amount of universality. This is verified by detailed numerical calculations.

03.75.-b, 03.75.Dg, 03.67.-a, 03.65.Ge

## I. INTRODUCTION

The duality between wave and particle aspects is one of the central issues of Quantum Mechanics. Much has been made of the particle aspects of photons, but the recent progress in cooling and controlling atomic motion has brought forward their wave mechanical behavior in a prominent way. The new field of Atomic Optics has emerged [1].

With modern cooling and trapping techniques, one can envisage controlled motion of atomic particles in structures whose mechanical dimensions match the heterostructures used in electronic circuits. Neutral atoms can be stored in magneto-optical traps, and Hänsch and his group has recently shown [2] that such traps can be made very small, *viz* of the order of  $10^2 \mu\text{m}$ . This requires high precision in the fabrication of the solid structures defining the dimensions of the trap. Modern lithographic technology suggests that such structures could be made even much smaller, and then we can imagine experiments in traps of genuinely microscopic dimensions, where quantum effects would dominate the particle dynamics. Hänsch has also suggested that such traps could be made into channels and structures, thus providing a tool to design arbitrary devices at the surface of a substrate.

Similar structures can be constructed by combining charged wires with evanescent wave mirrors [3,4] or magnetic mirrors [5]. Such combinations can be used to build up the structures utilized in nano-electronics. The use of wires to guide atomic motion has been investigated by Denschlag and Schmiedmayer [6]. Schmiedmayer has also discussed the use of such structures to construct quantum dots and quantum wires for atoms [7].

Alternative ways to achieve guided motion and possibly controlled interaction between atoms is to utilize hollow optical fibers with evanescent waves trapping the atoms to narrow channels at the center of the fiber [8,9]. These can eventually be fused to provide couplers similar to those used for optical signal transmission in fibers. Also the pure atomic waveguide achievable by the use of hollow laser modes may be used.

We see these methods as an opening to novel and innovative uses of particle traps. By arranging a network of grooves on a surface, we can launch particles (wave packets) into the various inputs of the system, let them propagate through the device and interact with its structures and each other. This may well provide an opportunity to design quantum apparatuses, process information and perform computations. The advantage is that both the structures and the input states are easy to control in an atomic environment. An equivalent point of view is expressed by Schmiedmayer in Ref. [7].

A next step in the experimental progress would be to observe the quantum character of atoms (or possibly ions). An essential quantum characteristic of particles is their statistical behavior. The difference between bosons and fermions manifests itself dramatically in many situations. Optical networks can be fed by a few photons only, and their quantum aspects have been utilized in experiments ranging from secure communication to tests of fundamental issues. Recently Zeilinger and his group [10] have tested the behavior of two-photon states at beam splitters. Using the overall symmetry properties of the states, they have been able to display both symmetric and antisymmetric behavior.

Similar experiments are in principle possible with electrons. In nanostructures, one can fabricate the devices simulating optical components, but it is far less trivial to launch single conduction electrons in well controlled states. Yamamoto's group, however, has been able to show quantum correlations in an experiment which is the analogue of a beam splitter for photons [11].

In this paper we give an example of the multiparticle effects observable when particle states are launched along potential grooves on a surface. The specific phenomenon singled out for investigation is the effect of particle statistics

at a beam-splitter-like coupling device. The corresponding effect with photons is described in Sec. II as a motivation. In Sec. III we present the details of the model chosen and a simplified analytic treatment demonstrating the main features expected of this model. In Sec. IV we carry through a numerical analysis of the situation, for one particle as a two-dimensional propagation problem, but for two particles in a paraxial approximation. For non-interacting particles, the expected behavior is found, but when particle interactions are added, the boson behavior is changed. For fermions the exclusion principle makes them essentially insensitive to the interaction. An unexpected feature is found: the sign of the interaction is irrelevant for the effect. In Sec. V this is explained within our simple analytic model, and, as a consequence, a certain universality is proposed: When the interaction strength over the tunneling frequency becomes of the order of  $\sqrt{3}$ , the noninteracting bosonic behavior is essentially destroyed. This is verified by numerical calculations, reported in Fig. 13. Finally Sec. VI presents a discussion of parameter ranges in real materials, where our effects may be observable, and summarizes our conclusions.

## II. MOTIVATION

In order to show the opportunities offered by atomic networks, we investigate the manifestations of quantum statistics on an experiment emulating the behavior of photons in beam splitters. This is a straightforward approach, which enables us to display the potentialities and limitations of such treatments.

Our work has been motivated by the statistics displayed by a 50-50 beam splitter, which has been used in the experiments by the Zeilinger group [10]. When two particles are directed into the beam splitter in the incoming modes in Fig. 1, they are piloted into the outgoing modes according to the beam splitter relations

$$\begin{bmatrix} a_{\text{out}}^\dagger \\ b_{\text{out}}^\dagger \end{bmatrix} = \frac{1}{\sqrt{2}} \begin{bmatrix} 1 & -i \\ -i & 1 \end{bmatrix} \begin{bmatrix} a_{\text{in}}^\dagger \\ b_{\text{in}}^\dagger \end{bmatrix}; \quad (1)$$

see Ref. [12]. When one particle is directed into each incoming channel, the state is

$$|\Psi\rangle = a_{\text{in}}^\dagger b_{\text{in}}^\dagger |0\rangle, \quad (2)$$

where  $|0\rangle$  is the vacuum state. Without assuming anything about the statistics of the incoming particles, we can express the state (2) in terms of the outgoing states by inverting the relation (1) as

$$|\Psi\rangle = \frac{i}{2} \left[ \left( a_{\text{out}}^\dagger \right)^2 + \left( b_{\text{out}}^\dagger \right)^2 \right] |0\rangle + \frac{1}{2} \left[ a_{\text{out}}^\dagger, b_{\text{out}}^\dagger \right] |0\rangle. \quad (3)$$

From this follows that boson statistics gives

$$|\Psi\rangle = \frac{i}{\sqrt{2}} (|n_{a,\text{out}} = 2, n_{b,\text{out}} = 0\rangle + |n_{a,\text{out}} = 0, n_{b,\text{out}} = 2\rangle); \quad (4)$$

the particles emerge together at either output. For fermions we have

$$\begin{aligned} |\Psi\rangle &= a_{\text{out}}^\dagger b_{\text{out}}^\dagger |0\rangle \\ &= |n_{a,\text{out}} = 1, n_{b,\text{out}} = 1\rangle, \end{aligned} \quad (5)$$

and they always remain separated.

Weihs et al. [10] have been able to verify these properties experimentally using photons. As the requirements of quantum statistics refer only to the total wave functions, they have been able to realize both the symmetric and the antisymmetric case, thus offering the behavior of both bosons and fermions.

Photons are ideal for experiments, they do not interact mutually and they propagate essentially undisturbed in vacuum. As models for quantum systems, they have the drawback that they cannot be localized, their wave packets are of rather elusive character, and the influence of particle interactions cannot be established. Thus we have chosen to discuss the propagation of massive particles through beam-splitter-like structures. As explained above, such experiments may be performed with atoms or electrons in traps of microscopic dimensions. We can thus investigate the propagation of wave packets through these structures, explore the role of quantum statistics and switch on and off the particle interaction at will.

### III. THE MODEL

We consider particles moving in potential wells which form grooves over a two-dimensional surface. These may cross or couple by tunneling when approaching each other, thus forming a network of potential channels emulating a linear optical system.

Here we consider two separate channels which run parallel for  $z \rightarrow \pm\infty$  and approach each other in the  $x$ -direction, as shown in Fig. 2. For simplicity we construct the potential from two harmonic oscillators

$$U_{\pm}(x) = \frac{1}{2}m\omega^2(x \pm \frac{1}{2}d)^2, \quad (6)$$

so that a double well potential can be obtained by writing

$$\begin{aligned} U(x, z) &= \frac{U_+(x, z)U_-(x, z)}{U_+(x, z) + U_-(x, z)} \\ &= \frac{1}{2}m\omega^2 \frac{(x + \frac{1}{2}d(z))^2 (x - \frac{1}{2}d(z))^2}{(x + \frac{1}{2}d(z))^2 + (x - \frac{1}{2}d(z))^2}. \end{aligned} \quad (7)$$

If we now choose  $d(z)$  in a suitable manner, we can achieve the potential behavior shown in Fig. 2. Note that at the minima, the potential  $U(x, z)$  essentially follows the shape of the smaller potential  $U_{\pm}$ .

We consider a wave packet sitting stationary near the bottom of one well at  $z = 0$ , where the distance between the wells is at its minimum  $d_0$ . The particle can then tunnel across the barrier with the rate

$$T \sim \exp \left[ - \int \sqrt{2mU(x, 0)} dx \right] \approx \exp \left[ -\kappa \sqrt{U(0, 0)} d_0 \right], \quad (8)$$

where  $\kappa$  is some constant. From Eq. (7) we see that  $U(0, 0) \propto d_0^2$  so that we expect

$$\log T \sim -\kappa' d_0^2 + \text{const.} \quad (9)$$

In order to acquire a heuristic understanding of the physics involved in the coupling of the grooves at  $z = 0$ , we look at the lowest eigenfunctions of the double well potential. These are expected to be symmetric,  $\psi_S$ , with energy  $E_S$ , and antisymmetric,  $\psi_A$ , with energy  $E_A$ , as shown in Fig. 3. We have  $E_A > E_S$  and hence we write

$$\begin{aligned} E_A &= \overline{E} + \hbar\Omega \\ E_S &= \overline{E} - \hbar\Omega, \end{aligned} \quad (10)$$

where  $2\Omega$  is the tunneling frequency.

Using the eigenstates we form the localized states

$$\begin{aligned} \varphi_L &= \frac{1}{\sqrt{2}}(\psi_S + \psi_A) \\ \varphi_R &= \frac{1}{\sqrt{2}}(\psi_S - \psi_A), \end{aligned} \quad (11)$$

where the subscripts  $L$  ( $R$ ) denote left (right) localization.

We can easily integrate the time evolution by using the energy eigenstates. If we now assume that we start from  $\varphi_L$  at time  $t = 0$ , then

$$\begin{aligned} \Psi(t) &= \exp(-iHt/\hbar) \varphi_L \\ &= \frac{1}{\sqrt{2}} \exp(-i\overline{E}t/\hbar) (e^{i\Omega t} \psi_S + e^{-i\Omega t} \psi_A) \\ &= \exp(-i\overline{E}t/\hbar) (\cos \Omega t \varphi_L + i \sin \Omega t \varphi_R). \end{aligned} \quad (12)$$

This displays the expected flipping back and forth between the two wells. For

$$\Omega t_0 = \frac{\pi}{4} \quad (13)$$

the coupling performs the action of a 50-50 beam splitter.

We now move to consider the action of such a potential configuration on a two particle initial state. We first choose the bosonic one

$$\Psi_0^B = \frac{1}{\sqrt{2}} (\varphi_L(1)\varphi_R(2) + \varphi_L(2)\varphi_R(1)), \quad (14)$$

where the argument denotes the coordinates of the particle. This can be expressed as

$$\Psi_0^B = \frac{1}{\sqrt{2}} (\psi_S(1)\psi_S(2) - \psi_A(1)\psi_A(2)), \quad (15)$$

which can be evolved in time straightforwardly to give

$$\begin{aligned} \exp(-iHt_0/\hbar) \Psi_0^B &= \frac{1}{\sqrt{2}} \exp(-i2\bar{E}t_0/\hbar) (e^{i2\Omega t_0} \psi_S(1)\psi_S(2) - e^{-i2\Omega t_0} \psi_A(1)\psi_A(2)) \\ &= \frac{i}{\sqrt{2}} \exp(-i2\bar{E}t_0/\hbar) (\varphi_L(1)\varphi_L(2) + \varphi_R(2)\varphi_R(1)). \end{aligned} \quad (16)$$

As we see, the bosonic two particle state works as in Eq. (4): both particles emerge together.

In the fermionic case we have

$$\begin{aligned} \Psi_0^F &= \frac{1}{\sqrt{2}} (\varphi_L(1)\varphi_R(2) - \varphi_L(2)\varphi_R(1)) \\ &= \frac{1}{\sqrt{2}} (\psi_A(1)\psi_S(2) - \psi_S(1)\psi_A(2)). \end{aligned} \quad (17)$$

Because both states  $\psi_A\psi_S$  and  $\psi_S\psi_A$  evolve with the energy  $2\bar{E}$ ,  $\Psi_0^F$  remains uncoupled to other states. Thus the fermions emerge at separate exit channels as expected.

## IV. NUMERICAL WORK

### A. The Schrödinger equation

The Schrödinger equation in the two-dimensional system is of the form

$$i\hbar \frac{\partial}{\partial t} \Psi(x, z, t) = \left[ -\frac{\hbar^2}{2m} \left( \frac{\partial^2}{\partial x^2} + \frac{\partial^2}{\partial z^2} \right) + U(x, z) \right] \Psi(x, z, t). \quad (18)$$

As a preparation for the numerical work, we introduce the scaling parameters  $\tau$  and  $\xi$  giving the dimensionless variables

$$\begin{aligned} \tilde{x} &= x/\xi \\ \tilde{z} &= z/\xi \\ \tilde{t} &= t/\tau \\ \tilde{p} &= \tau p/m\xi. \end{aligned} \quad (19)$$

We apply this to the one-dimensional oscillator Hamiltonian

$$H = \frac{p^2}{2m} + \frac{1}{2}m\omega^2 x^2 \quad (20)$$

and find the Schrödinger equation

$$i \left( \frac{\hbar\tau}{m\xi^2} \right) \frac{\partial}{\partial \tilde{t}} \Psi = \left( \frac{\tilde{p}^2}{2} + \frac{1}{2}\tilde{\omega}^2 \tilde{x}^2 \right) \Psi. \quad (21)$$

The dimensionless oscillator frequency is given by  $\tilde{\omega} = \omega\tau$ . This shows that choosing the scaling units suitably, we can tune the effective dimensionless Planck constant

$$\tilde{\hbar} = \frac{\hbar\tau}{m\xi^2}. \quad (22)$$

To check the consistency of this we calculate

$$[\tilde{x}, \tilde{p}] = \left(\frac{1}{\xi}\right) \left(\frac{\tau}{m\xi}\right) [x, p] = i\tilde{\hbar}. \quad (23)$$

This gives us a way of controlling the quantum effects in the numerical calculations.

In our numerical calculations we employ the split operator method [13]

$$\exp[-i(T+U)\Delta t/\hbar] \approx \exp[-iT\Delta t/\hbar] \exp[-iU\Delta t/\hbar]. \quad (24)$$

The corrections to this are given by

$$[T, U] \frac{\Delta t^2}{2\hbar^2} = \left| \left( \frac{\tilde{\Delta t}^2 \tilde{\omega}^2}{4} \right) \left( \frac{\tilde{x}\tilde{p} + \tilde{p}\tilde{x}}{\tilde{\hbar}} \right) \right|. \quad (25)$$

In order to achieve satisfactory numerical accuracy, this should not be too large; in our calculations, with  $\Delta t = 0.001$ ,  $\tilde{\omega} = 30$  and  $\tilde{\hbar} = 6$  the expectation value of expression (25) is of the order of  $10^{-4}$ . Decreasing  $\Delta t$  or the grid spacing has been found not to change our results significantly.

In the following discussion, we use the scaled variables, but for simplicity, we do not indicate this in the notation. Whenever variables are assigned dimensionless values, these refer to the scaled versions.

In order to achieve beam splitter operation, we let the distance between the potential wells vary in the following way

$$d(z) = 2 + d_0 - \frac{2}{\cosh(z/\eta)}, \quad (26)$$

which inserted into Eq. (7) gives a potential surface as shown in Fig. 2. To test its operation as beam splitter, we let a wave packet approach the coupling region in one of the channels, and follow its progress through the intersection numerically as a two-dimensional problem. The result is shown in Fig. 4. We see that the parameters chosen lead to ideal 50-50 splitting of the incoming wave packet. The progress of the wave packet through the interaction region is steady and nearly uniform, and no backscattering is observed. This suggest simplifying the situation so that the motion in the  $z$ -direction is replaced by a constant velocity, and the full quantum problem is computed only in the  $x$ -direction. If the wave packet is long enough in the  $z$ -direction, its velocity is well defined, and this should be a good approximation.

The implementation of such a paraxial approach becomes imperative when we want to put two particles into the structure. The full two-dimensional integration would require the treatment of four degrees of freedom, which is demanding on the computer resources. With the paraxial approximation, two particles can be treated by a two-dimensional numerical approach, which is within the resources available.

To introduce the paraxial approximation, we perform a Galilean transformation of the wave function to a co-moving frame

$$\psi(x, z, t) = \varphi(x, \varsigma, t) \exp \left[ \frac{i}{\hbar} \left( p_0 z - \frac{p_0^2 t}{2m} \right) \right], \quad (27)$$

where

$$\varsigma = z - \frac{tp_0}{m}. \quad (28)$$

The initial momentum in the  $z$ -direction is denoted by  $p_0$ . The new wave function is found to obey the Schrödinger equation

$$i\hbar \frac{\partial}{\partial t} \varphi(x, \varsigma, t) = \left[ -\frac{\hbar^2}{2m} \left( \frac{\partial^2}{\partial x^2} + \frac{\partial^2}{\partial \varsigma^2} \right) + U \left( x, \varsigma + \frac{tp_0}{m} \right) \right] \varphi(x, \varsigma, t). \quad (29)$$

For a well defined momentum  $p_0$ , the wave packet is very broad in the  $\varsigma$ -direction and its derivatives with respect to  $\varsigma$  may be neglected. The corresponding degree of freedom disappears, and it is replaced by a potential sweeping by with velocity  $p_0/m$ . This is what we call the paraxial approximation.

Taking the parameters from the integration in Fig. 4, we can obtain the beam splitting operation also in the paraxial approximation as shown in Fig. 5. The transfer of the wave packet from one well to the linear superposition is shown in Fig. 6. This proves that the potential configuration works exactly as in the analytic result (12).

Now the integration is one-dimensional for a single particle, and it is easy to investigate the tunneling probability as a function of the parameters. In Fig. 7 we display the transition rate  $T$  as a function of the parameter  $d_0^2$ , which controls the coupling between the wells. For small values,  $d_0^2 < 3$ , we are in a coherent flipping region; the wave packet is transferred back and forth between the wells and resonant transmission occurs. For larger values,  $d_0^2 > 3$ , the analytic estimate of a logarithmic dependence in Eq. (9) is seen to hold approximately. Our calculations work at  $d_0 = 1.8903$ , which gives  $T = 1/2$ .

## B. Effects of quantum statistics

We can now integrate the propagation of a two-particle wave function by choosing the initial state to be combinations of

$$\varphi_{L(R)}^0(x) = N \exp \left[ -\frac{\omega}{2\hbar} \left( x \pm \left( 1 + \frac{1}{2}d_0 \right) \right)^2 \right], \quad (30)$$

where the  $+$  ( $-$ ) refers to the particle entering in the left (right) channel. For bosons, this is used in the combination (14) and integrated in the potential (7), where the  $z$ -dependence is replaced by a  $t$ -dependence according to Eq. (29). The result is shown in Fig. 8. At  $t = -10$ , the bosons enter symmetrically in the two input channels, i.e. they have different signs for their coordinates. After being mixed at time  $t = 0$ , they emerge together with equal strength at both output channels, i.e. their coordinates have the same sign. This result fully reproduces the behavior expected from bosons at a 50-50 beam splitter.

We can, however, also test the fermionic case by using the state (17) as the initial one. The result is shown in Fig. 9. Near  $t = 0$ , the wave packets follow the potential wells, but they remain separated and emerge at different outputs as expected. Fermions do not like to travel together.

We have thus been able to verify the properties of a 50-50 beam splitter on massive particles represented by wave packets travelling in potential structures. The calculations in Figs. (8) and (9) do not, however, include any particle interactions. We can now proceed to include these, and evaluate their effect on the manifestations of quantum statistics.

When we introduce the interaction, we have to decide which type of physical system we have in mind. Conduction electrons or ions interact through the Coulomb force whereas neutral atom interactions may be described by a force of the Lennard-Jones form. In both cases, the interaction is singular at the origin, and it has to be regularized there. We do this by introducing the variable

$$r_\varepsilon = \sqrt{r^2 + \varepsilon^2}. \quad (31)$$

This makes the interaction energy finite when the particles overlap, but does not affect the main part of our argument in other ways.

With this notation the Coulomb interaction is written

$$V_C(r) = \frac{V_0}{r_\varepsilon}, \quad (32)$$

and the Lennard-Jones interaction is

$$V_{LJ}(r) = V_0 \left[ \left( \frac{b}{r_\varepsilon} \right)^{12} - \left( \frac{b}{r_\varepsilon} \right)^6 \right]; \quad (33)$$

this contains the additional range parameter  $b$ . In both cases, the strength of the interaction is regulated by  $V_0$ .

It is straightforward to integrate the Schrödinger equation with the two-particle interaction included, and look how its increase affects the correlations imposed by quantum statistics. For fermions, the effect is essentially not seen in the parameter ranges we are able to cover. As seen from Fig. 9, the particles never really approach each other, and they remain separated due to their quantum statistics for all times; the interaction does not affect them.

For bosons the effect is different. We have investigated their behavior for a range of interaction parameters and find that an increase in the interaction does destroy the simple behaviors found for noninteracting ones. The result of

such an integration is found in Fig. 10. Compared with Fig. 8 this shows that now the particles appear in separate channels with about the same probability as in the same channels. Thus the statistical effect has been destroyed. Fig. 11 shows how the result emerges during the time evolution; the system tries to achieve the ideal case, but settles to the final state observed in Fig. 10.

Figure 12 shows how an increase in the interaction strength destroys the ideal behavior. This is drawn using a Lennard-Jones potential, but the behavior is similar for other cases we have investigated.

One unexpected feature emerged from our calculations: The destruction of the ideal behavior turned out to be independent of the sign of the interaction. One may have expected an attractive interaction between the bosons to enhance their tendency to appear together, but this turned out not to be the case. In order to understand this feature we have to turn to our simple analytic argument in Sec. III and investigate the interplay between two-particle states and the interaction.

## V. STATISTICS VERSUS INTERACTIONS

In order to introduce the particle interaction, we choose a convenient basis for the two-particle states. As the first component we choose the bosonic state (14)

$$u_1 = \frac{1}{\sqrt{2}} (\varphi_L(1)\varphi_R(2) + \varphi_L(2)\varphi_R(1)). \quad (34)$$

In addition, there are two more bosonic states, where the particles enter in the same channels

$$u_2 = \frac{1}{\sqrt{2}} (\varphi_L(1)\varphi_L(2) + \varphi_R(2)\varphi_R(1)) \quad (35)$$

$$= \frac{1}{\sqrt{2}} (\psi_A(1)\psi_A(2) + \psi_S(1)\psi_S(2)) \quad (36)$$

and

$$u_3 = \frac{1}{\sqrt{2}} (\varphi_L(1)\varphi_L(2) - \varphi_R(2)\varphi_R(1)) \quad (37)$$

$$= \frac{1}{\sqrt{2}} (\psi_S(1)\psi_A(2) + \psi_A(1)\psi_S(2)).$$

As the last component we have the fermionic basis function (17)

$$u_4 = \frac{1}{\sqrt{2}} (\varphi_L(1)\varphi_R(2) - \varphi_L(2)\varphi_R(1)). \quad (38)$$

Together the functions  $\{u_i\}$  form a complete Bell state basis for the problem. They are also convenient for the introduction of particle interactions. In the states  $u_1$  and  $u_4$  the wave functions overlap only little, and the effect of the interaction is small. For the states  $u_2$  and  $u_3$  they sit on top of each other and feel the interaction strongly. We treat this in a Hubbard-like fashion by saying that the energy of the latter states is changed by the value  $2\bar{V} \propto V_0$ . Because the overlap between  $\varphi_L$  and  $\varphi_R$  is small, we have  $(u_1, Vu_1) \approx (u_4, Vu_4)$  and  $(u_2, Vu_2) \approx (u_3, Vu_3)$ , and we can use the definition

$$2\bar{V} = \frac{1}{2} [(u_2, Vu_2) + (u_3, Vu_3) - (u_1, Vu_1) - (u_4, Vu_4)] \quad (39)$$

$$\approx \int \int \varphi(x)^2 \varphi(y)^2 V(|x-y|) dx dy - \int \int \varphi(x)^2 \varphi(y-d_0)^2 V(|x-y|) dx dy,$$

where  $V$  is either a Coulomb or Lennard-Jones interaction. The first terms give the effective interaction energy when both particles sit in the same potential groove. In the states  $u_1$  and  $u_4$  both grooves are occupied and because they are at their closest at  $z = 0$ , we subtract the mutual interaction energy across the separating barrier to obtain the pure local interaction energy. The second line results if we approximate both  $\varphi_L$  and  $\varphi_R$  by a Gaussian  $\varphi$  with the same width. From Eq. (16) we see that only the states  $u_1$  and  $u_2$  are coupled by the tunneling rate  $2\Omega$ . Thus if we express the state by

$$\Psi = a_1 u_1 + a_2 u_2 + a_3 u_3 + a_4 u_4, \quad (40)$$

the state vector  $[a_1, a_2, a_3, a_4]$  evolves with the Hamiltonian

$$\begin{bmatrix} 2\bar{E} & -2\hbar\Omega & 0 & 0 \\ -2\hbar\Omega & 2\bar{E} + 2\bar{V} & 0 & 0 \\ 0 & 0 & 2\bar{E} + 2\bar{V} & 0 \\ 0 & 0 & 0 & 2\bar{E} \end{bmatrix} = 2\bar{E} + \bar{V} + \begin{bmatrix} -\bar{V} & -2\hbar\Omega & 0 & 0 \\ -2\hbar\Omega & \bar{V} & 0 & 0 \\ 0 & 0 & \bar{V} & 0 \\ 0 & 0 & 0 & -\bar{V} \end{bmatrix}. \quad (41)$$

The constant part does not affect the coupling between the states, and the amplitudes  $a_3$  and  $a_4$  decouple. The remaining ones flip at the effective rate

$$\Omega_{\text{eff}} = \frac{1}{2} \sqrt{4\Omega^2 + \bar{V}^2 / \hbar^2}. \quad (42)$$

This result shows that the new parameter replacing  $\Omega$  in Eq. (10) is  $\Omega_{\text{eff}}$ , implying that the perfect boson behavior is expected to be destroyed for

$$\frac{\bar{V}}{2\hbar\Omega} \sim \sqrt{3} = 1.73. \quad (43)$$

This is in approximate agreement with the result shown in Fig. 12. By inspecting Fig. 11, we can also verify that the flipping does occur faster when we switch on the interaction, as expected from Eq. (42).

In the simplified analytic treatment, the only influence of the potential was through its strength  $|\bar{V}|$ . Hence we expect the results to scale with the parameter  $(|\bar{V}|/2\hbar\Omega)$  where  $2\hbar\Omega = E_A - E_S$ . The probability to emerge in the same output channels should essentially depend on this only; a certain universality is expected.

In Fig. 13, we have plotted this probability for a variety of potentials including both Coulomb and Lennard-Jones ones. As we can see, the behavior is very similar, at  $(|\bar{V}|/2\hbar\Omega) \approx 1.7$  the probability has decreased to less than 10% in agreement with our expectation. This verifies the degree of universality achieved. For comparison, we also used the simple analytic theory to obtain the points along the curve. In this treatment,  $2\Omega$  was assumed to be constant during some finite coupling time  $t$ , according to Eq. (13). By inspecting Fig. 6, we conclude that  $t$  should be of the order of unity. Here  $2\hbar\Omega$  was chosen to be 8, and the time evolution in the subspace  $\{u_1, u_2\}$  was calculated. This agrees best with the numerical results for small  $\bar{V}$ ; for larger values of  $\bar{V}$  the simple analytic treatment becomes invalid.

## VI. DISCUSSION AND CONCLUSIONS

The actual values of  $\xi$ ,  $\tau$ ,  $m$  and  $\omega$  depend on the physical system we have in mind. Our calculations are carried out at  $\tilde{\omega} = 30$  and  $\tilde{\hbar} = 6$ ; the momentum in the  $z$ -direction of the incoming wave packet is  $\tilde{p}_z = 30$  or  $\tilde{p}_z = 1000$ . If we consider an atomic beam splitter for Rb atoms, setting the length scale  $\xi$  to 100 nm corresponds to a time scale  $\tau$  of 80  $\mu\text{s}$  according to Eq. (22). A displacement of 400 nm from the center of one valley in the  $x$ -direction gives a potential energy increase of roughly 10 mK, i.e. a transverse velocity of 0.15 m/s. This is to be compared with a typical height of the confining potential in a hollow optical fiber, a few tens of mK [8,9]. Taking  $\tilde{p}_z = 1000$  yields a beam velocity of 1.3 m/s in the  $z$ -direction.

If we consider a mesoscopic electron beam splitter built on GaAs,  $\xi$  could be of the order of 40 nm, which means that the closest distance  $d_0$  between the valleys is 80 nm. This would correspond to  $\tau = 6$  ps, i.e. the electron goes through the device in a few picoseconds. With  $\tilde{p}_z = 30$ , the kinetic energy of the electron due to the motion in the  $z$ -direction would be of the order of 0.01 eV. A displacement of 100 nm from the center of one valley in the  $x$ -direction corresponds to a potential energy increase of roughly 0.05 eV, in comparison with the bandgap in GaAs, 0.115 eV.

The parameter ranges chosen in our illustrative computations may not be experimentally optimal, but they indicate that the effects are not totally outside the range of real systems. Even if our calculations are based on a rather simplified model, we find them suggesting effects possible in realistic setups. The main problem is to prepare the appropriate quantum states, launch them into the structures and retain their quantum coherence during the interaction. With atomic cooling and trapping techniques, this may be feasible in the near future. For electrons the possibility to retain quantum coherence is still an open question.

We have chosen to discuss the straightforward question of particle statistics at a beam splitter. This is a simple situation, which, however, presents genuine quantum features. For information processing and quantum logic slightly more complicated networks are needed. Simple gate operation can be achieved along the lines described in Ref. [14], which was formulated in terms of conduction electrons, but similar situations can be envisaged for interacting atoms.

In this paper we suggest an analytic model, which can be used to analyze the behavior of particle networks confined to potential grooves in two-dimensional structures as discussed also by Schmiedmayer [7]. For complicated situations, the full numerical treatment rapidly becomes intractable and simplified qualitative tools are needed. We hope to have contributed to the development of such methods in the present paper.



## ACKNOWLEDGMENTS

One of us (SS) thanks Dr. Jörg Schmiedmayer for inspiring discussions. MTF thanks Patrick Bardroff for fruitful discussions.

- 
- [1] C. S. Adams, M. Siegel, and J. Mlynek, Phys. Rep. **240**, 143 (1994).
  - [2] V. Vuletic, T. W. Hänsch, and C. Zimmermann, Europhysics Letters **36**, 349 (1996).
  - [3] T. Esslinger, M. Weidemüller, A. Hennerich, and T. Hänsch, Opt. Lett. **18**, 450 (1993).
  - [4] W. Seifert, R. Kaiser, A. Aspect, and J. Mlynek, Opt. Comm. **111**, 566 (1994).
  - [5] T. M. Roach, H. Abele, M. G. Boshier, H. L. Grossman, K. P. Zetie, and E. A. Hinds, Phys. Rev. Lett. **75**, 629 (1995); I. C. Hughes, P. A. Barton, T. M. Roach, M. G. Boshier, and E. A. Hinds, J. Phys. B. **30**, 647 (1997).
  - [6] J. Denschlag and J. Schmiedmayer, Europhys. Lett. **38**, 405 (1997).
  - [7] J. Schmiedmayer, Eur. Phys. J. D **4**, 57 (1998).
  - [8] H. Ito, T. Nakata K. Sakaki, M. Ohtsu, K. I. Lee, and W. Jhe, Phys. Rev. Lett. **76**, 4500 (1998).
  - [9] J. Yin, Y. Zhu, W. Wang, Y. Wang, and W. Jhe, J. Opt. Soc. Am. B **15**, 25 (1998).
  - [10] G. Weihs, M. Reck, H. Weinfurter, and A. Zeilinger, Phys. Rev. Lett. **54**, 893 (1996); K. Mattle, H. Weinfurter, P. Kwiat, and A. Zeilinger, *ibid.* **76**, 4656 (1996).
  - [11] R. C. Liu, B. Odom, Y. Yamamoto and S. Tarucha, Nature **391**, 263 (1998).
  - [12] U. Leonhardt, *Measuring the Quantum State of Light*, Cambridge University Press, Cambridge (1997).
  - [13] J. A. Fleck, J. A. Morris, and M. D. Feit, Appl. Phys. **10**, 129 (1976); M. D. Feit, J. A. Fleck, and A. Steiger, J. Comput. Phys. **47**, 412 (1982).
  - [14] M. Kira, I. Tittonen, and S. Stenholm, Phys. Rev. B **52**, 10972 (1995).

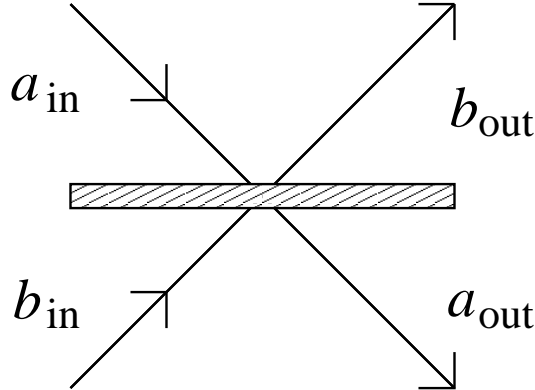


FIG. 1. Schematic drawing of a beam splitter. The incoming modes  $a_{\text{in}}, b_{\text{in}}$  are piloted into the outgoing modes  $a_{\text{out}}, b_{\text{out}}$  according to the beam splitter relations.

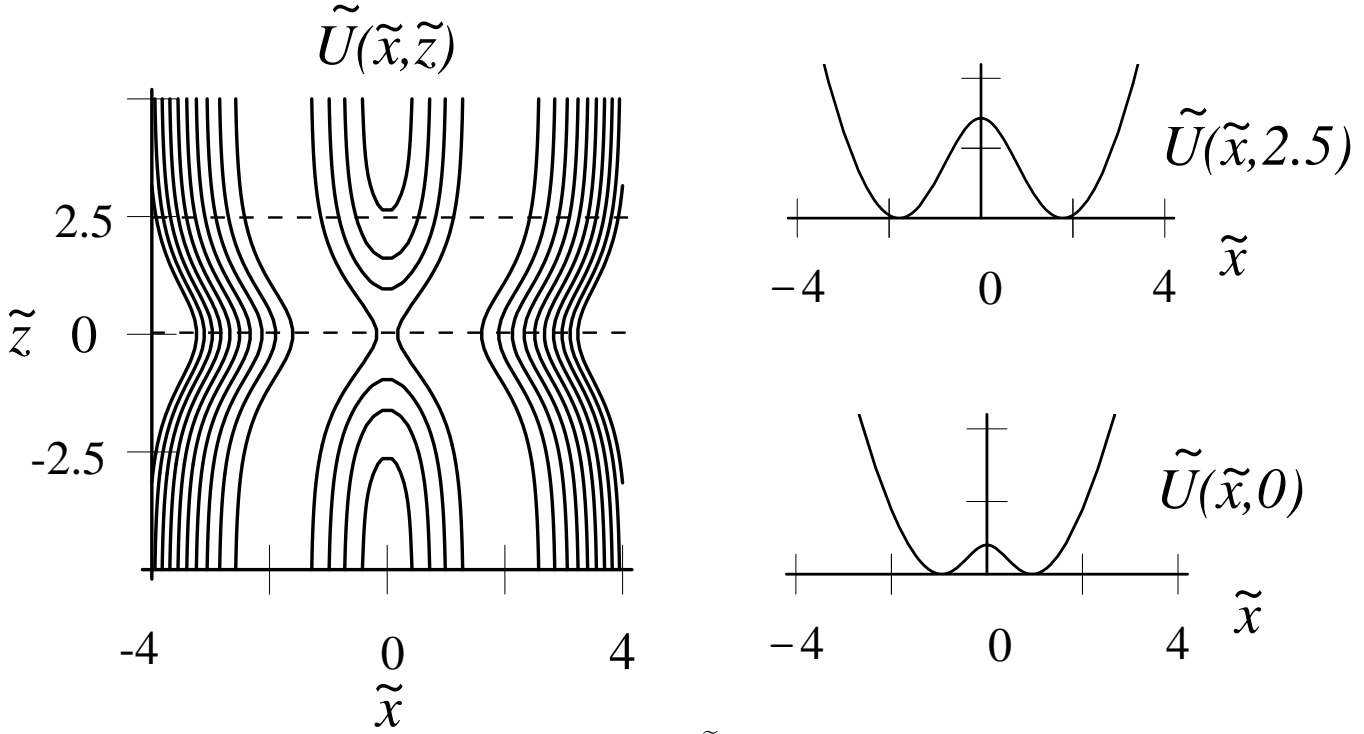


FIG. 2. A contour plot of the beam splitter potential  $\tilde{U}(\tilde{x}, \tilde{z})$ . The two channels approach each other at  $\tilde{z} = 0$ . The scaled variables  $\tilde{x}$  and  $\tilde{z}$  used in the numerical calculations are related to  $x$  and  $z$  according to Eq. (19). The scaled dimensionless oscillator frequency is  $\tilde{\omega} = 30$ . The distance  $d(\tilde{z})$  between the two valleys is chosen as in Eq. (26), with  $d_0 = 1.8903$  and  $\eta = 1$ . Two cross sections of the potential at  $\tilde{x} = 0$  and  $\tilde{x} = 2.5$  are also shown.

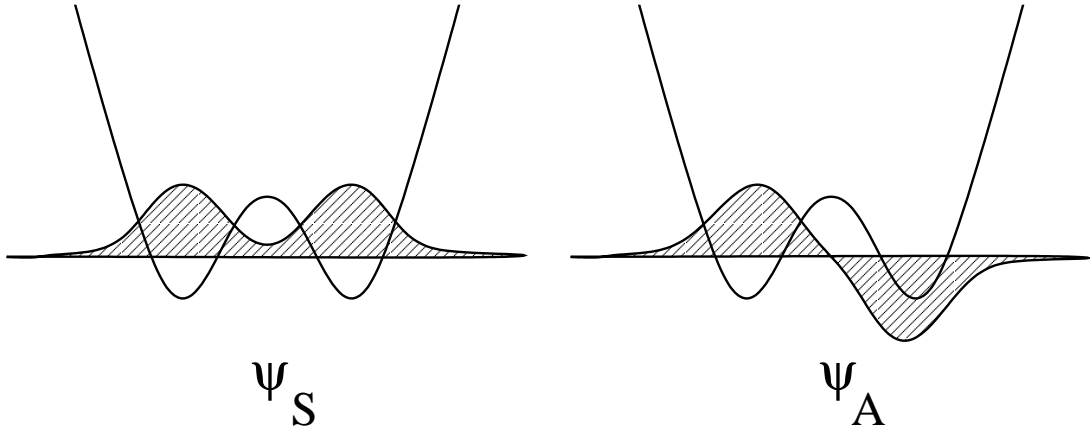


FIG. 3. Symmetric and antisymmetric eigenfunctions  $\psi_S$  and  $\psi_A$  of the double well.

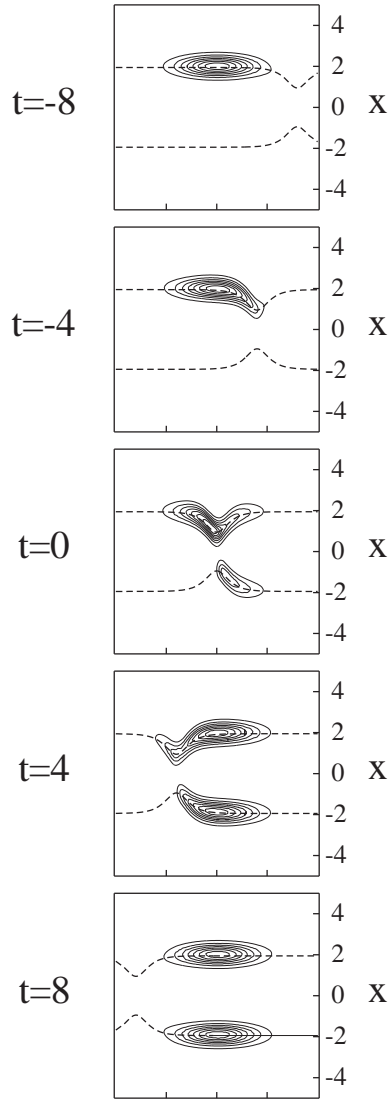


FIG. 4. Time evolution of a two-dimensional Gaussian wave packet propagating through the 50-50 beam splitter. The frame shown is centered around the wave packet moving in the  $z$ -direction. The dashed lines represent the minima of the potential. The potential is given by the scaled version of Eq. (7) with  $d(z)$  as in Eq. (26) where  $\eta = 30$ . The scaled oscillator frequency is  $\tilde{\omega} = 30$ ;  $\tilde{\hbar} = 6$ .

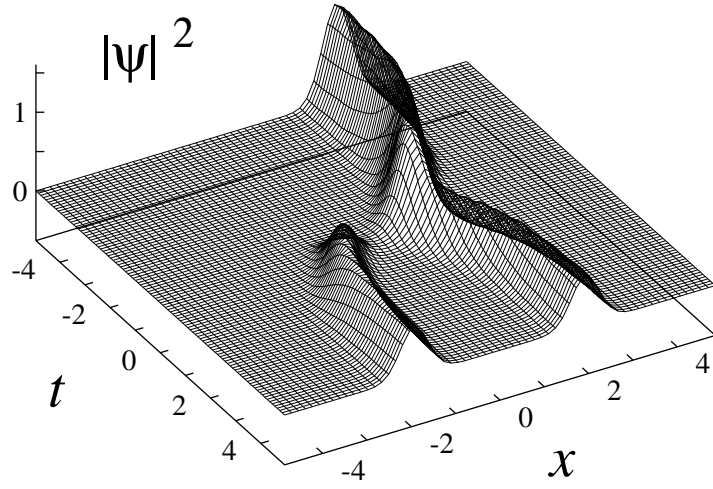


FIG. 5. Time evolution of a wave packet propagating through the 50-50 beam splitter in the paraxial approximation. The wave packet is incident in one channel and splits into two equal parts. Parameters are as in Fig. 4, the only difference is that in the potential  $U(x, z)$ ,  $z$  is replaced by  $tp_0/m$  according to the paraxial approximation. The initial wave packet is  $\varphi^0(x) = N \exp \left[ -\frac{\omega}{2\hbar} (x - (1 + d_0/2))^2 \right]$ .

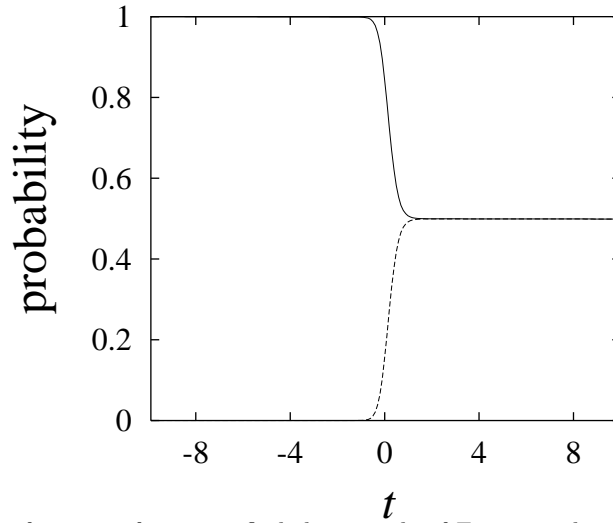


FIG. 6. The probabilities, as a function of time, to find the particle of Fig. 5 in the right (full line) and left (dashed line) valley of the beam splitter. The particle is incident at the right input and emerges with equal probability at the left and right outputs. Parameters as in Fig. 5.

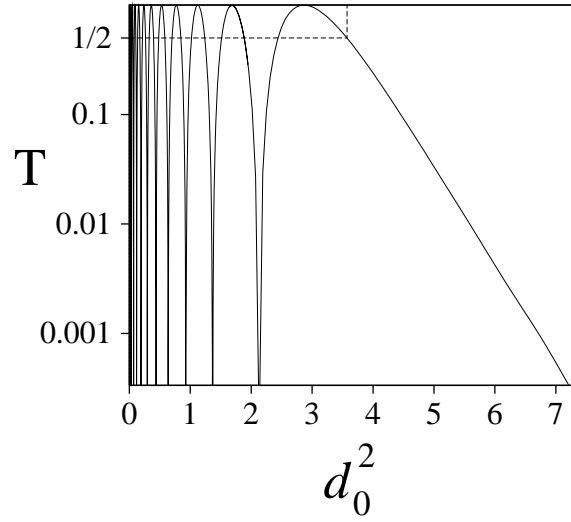


FIG. 7. Tunneling probability as a function of the square of the minimum distance between the valleys,  $d_0^2$ . The point of 50-50 beam splitter operation,  $d_0 = 1.8903$ , is indicated with dashed lines. For small values of  $d_0^2$ , the wave packet is transferred back and forth between the wells and resonant transmission occurs. For larger values,  $d_0^2 > 3$ , the relation (9) is seen to hold approximately.

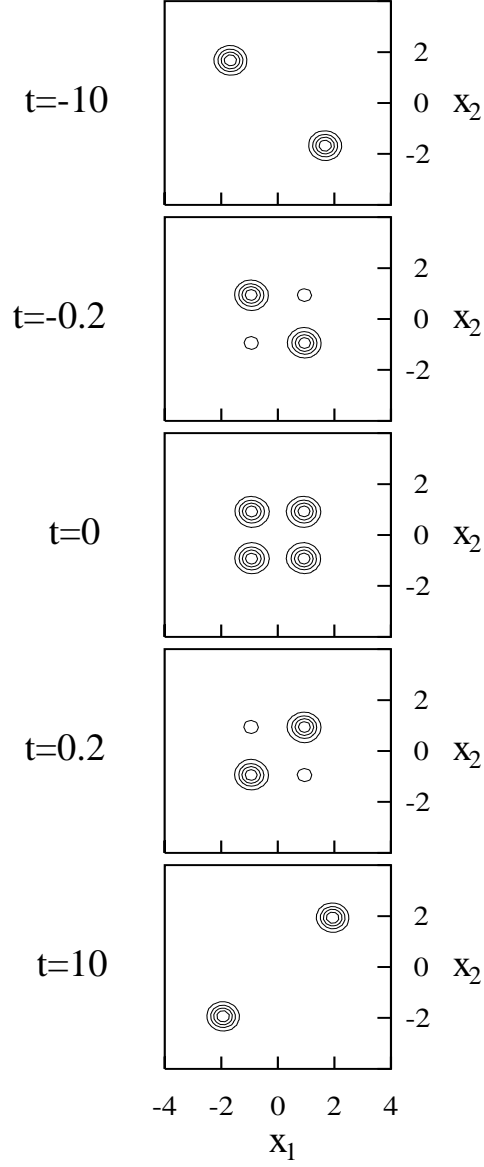


FIG. 8. Two bosons propagating through the beam splitter. Snapshots of the two-particle wave-function  $|\Psi|^2$  at different times are shown. On the horizontal axes we see the coordinate of particle 1; the vertical axes refer to particle 2. The two particles are seen incident in different input channels; they mix around  $t = 0$  and finally exit together. Parameters as in Fig. 5.

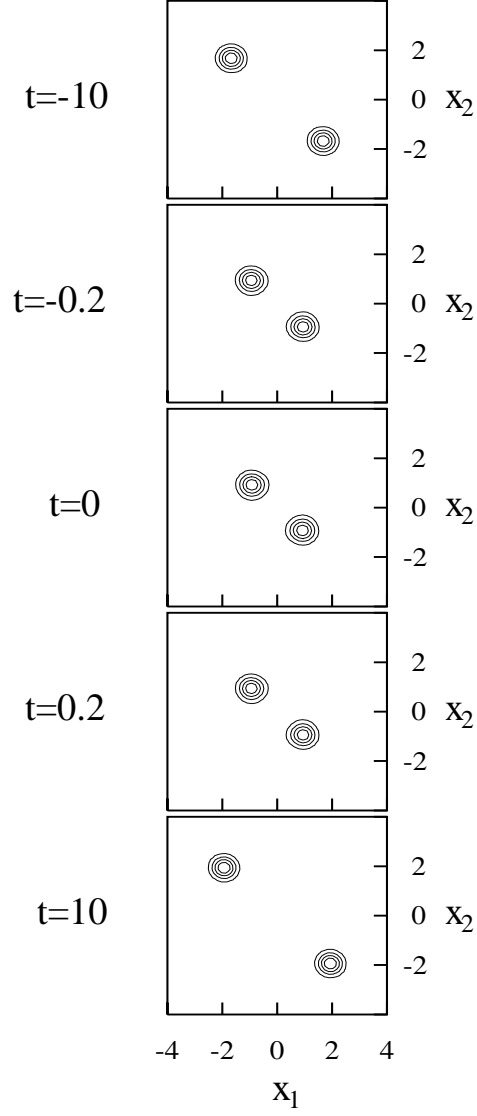


FIG. 9. Two fermions propagating through the beam splitter. Snapshots of the two-particle wave function  $|\Psi|^2$  at different times are shown. On the horizontal axes we see the coordinate of particle 1; the vertical axes refer to particle 2. The two particles enter and exit in different input and output channels. Parameters as in Fig. 5.

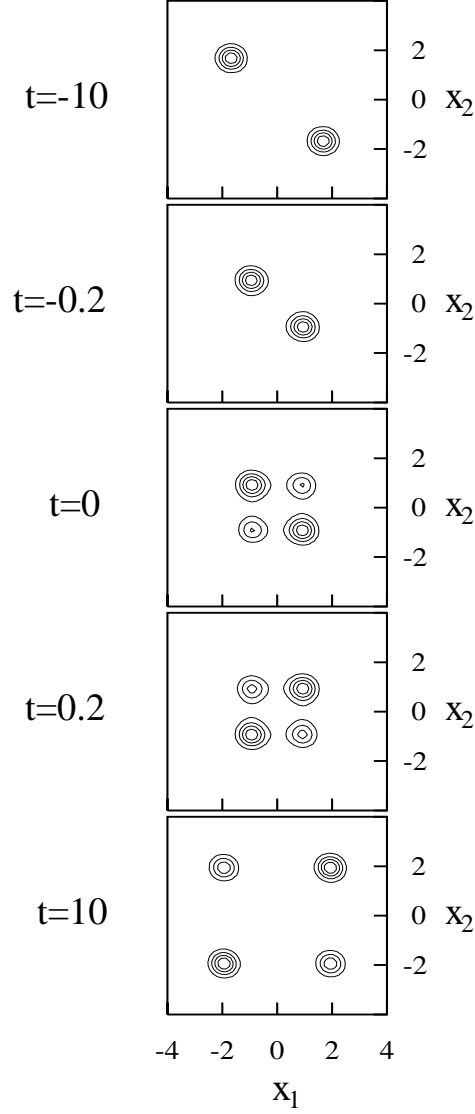


FIG. 10. Two bosons propagating through the beam splitter; interaction is included. Snapshots of the two-particle wave function  $|\Psi|^2$  at different times are shown. On the horizontal axes we see the coordinate of particle 1; the vertical axes refer to particle 2. The two particles enter in different input channels and mix around  $t = 0$ . With no interaction the two bosons were always emerging together, as in Fig. 8. Now there is a finite probability also for the bosons to emerge in separate output channels. The interaction is given by Eq. (32), with  $V_0 = 50$  and  $\varepsilon = 1$ . Other parameters as in Fig. 5.



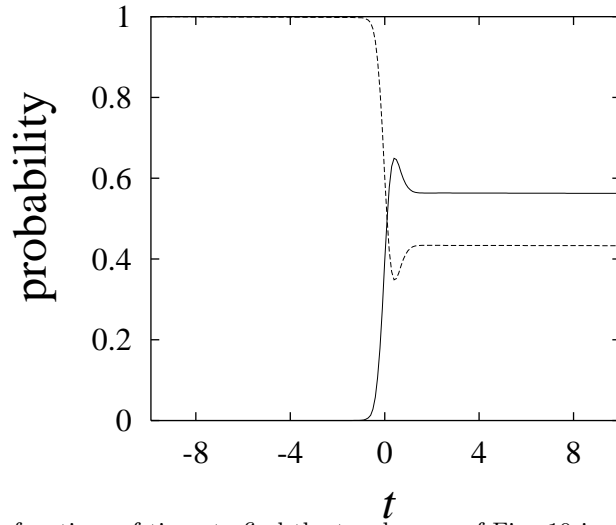


FIG. 11. The probabilities, as functions of time, to find the two bosons of Fig. 10 in different valleys (full line) and in the same valley (dashed line).

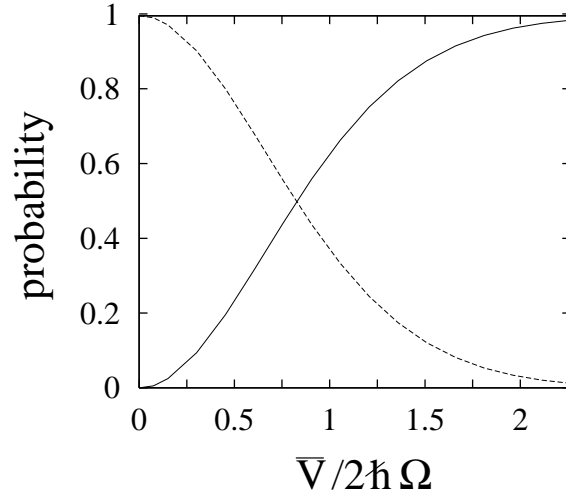


FIG. 12. The probabilities, as functions of interaction strength, for two bosons to emerge at different (full line) and same (dashed line) output channels. The Lennard-Jones interaction is given by Eq. (33), with  $b = 0.25$  and  $\varepsilon = 0.2$ . Parameters for the potential are as in Fig. 5.

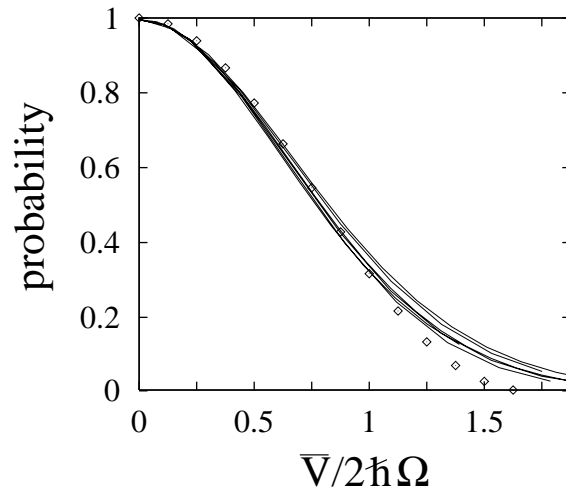


FIG. 13. The probability, as a function of interaction strength, for two bosons to emerge at the same output channel for several different types of interaction (full lines). We see that the perfect bosonic behavior is destroyed for  $\bar{V}/2\hbar\Omega \sim \sqrt{3} = 1.73$ . The parameter ranges are  $\varepsilon = 0.1$  to 1 for the Coulomb interaction and  $b = 0.25$  to 0.5,  $\varepsilon = 0.2$  to 0.35 for the Lennard-Jones interaction. The numerical results are compared with that of the analytic treatment (diamonds). In this model  $2\hbar\Omega$  was chosen to be 8, and the time evolution in the subspace  $\{u_1, u_2\}$  was calculated.